Mass-flux characteristics of tropical cumulus clouds from wind profiler observations at Darwin, Australia

Vickal V. Kumar

School of Mathematical Sciences, Monash University, Australia

Christian Jakob

School of Mathematical Sciences, Monash University, Australia and

ARC Centre of Excellence for Climate System Science, Monash University, Melbourne, Australia.

Alain Protat

Centre for Australian Weather and Climate Research: A partnership between the Bureau of Meteorology and CSIRO, Melbourne, Australia.

Christopher R. Williams

University of Colorado, and NOAA/Earth System Research Laboratory/Physical Sciences Division, Boulder, Colorado

Peter T. May

Centre for Australian Weather and Climate Research: A partnership between the Bureau of Meteorology and CSIRO, Melbourne, Australia.

Corresponding Author

Vickal V. Kumar

Centre for Australian Weather and Climate Research, Australian Bureau of Meteorology and CSIRO, GPO Box 1289, Melbourne 3001, Australia(E-mail: v.kumar@bom.gov.au)

Keywords: Wind profiler, congestus, deep clouds, overshooting clouds, relative moisture, cloud models

Abstract

Cumulus parameterizations in weather and climate models frequently apply mass-flux schemes in their description of tropical convection. Mass-flux constitutes the product of the fractional area covered by convection in a model grid box and the vertical velocity in the convective clouds. Vertical velocity is difficult to observe making the evaluation of mass-flux schemes difficult. Here, we combine high temporal resolution observations of the in-cloud vertical velocity over two wet-seasons at Darwin derived from a pair of wind profilers with the physical properties (cloud top heights CTH, convective-stratiform classification) of clouds derived from a C-band polarimetric radar to provide estimates of mass-flux and its components. The length of our data set also allows for investigations of the contributions to the overall mass-flux by different convective cloud types and of mass-flux variations with changes in the large-scale conditions. We found cumulus mass-flux was dominated by updrafts and in particular the updraft area fraction, with updraft vertical velocity playing a secondary role. The updraft vertical velocity peaked above 10 km where both the updraft area fraction and air density was minimal, resulting into a marginal effect on mass flux values. Downdraft area fractions are much smaller and velocities much weaker than those in updrafts. Area fraction responds very strongly to changes in mid-level large-scale vertical motion and changes in convective inhibition (CIN). In contrast, changes in the lower-troposphere relative humidity and convective available potential energy (CAPE) strongly modulate in-cloud vertical velocities but have moderate impacts on area fractions. Although average mass-flux is found to increase with increasing cloud top height it is environmental conditions that dictate the magnitude of mass-flux produced by deep convection through a combination of effects on area fraction and velocity.

1. Introduction

Cumulus clouds play an important role in weather and climate by maintaining the large-scale atmospheric circulation (e.g., Fritsch 1975; Emanuel et al. 1994), transporting heat, moisture, and momentum in the atmosphere (Yanai et al. 1973) and producing a multitude of clouds (e.g., Liu and Zipser, 2005). Recent studies indicate the existence of distinct types of cumulus clouds in the tropics (e.g. Johnson et al. 1999; Kumar et al. 2013a). These are shallow cumulus with cloud-top heights (CTH) near the trade inversion layer 1–3 km above the surface, mid-level cumulus congestus clouds with CTH near the 0°C freezing level (FZL), deep cumulonimbus clouds with CTH between FZL and tropopause layer, and overshooting convection with tops extending into the tropopause layer.

Individual cumulus clouds, particularly deep and overshooting modes, are generally thought to contain convective-scale (1–10 km) updraft and downdraft cores. Observations reveal that cumulus updraft and downdraft flow characteristics differ in several ways (e.g., Knupp and Cotton 1985). Updrafts are triggered by convergence of environmental airflow and typically start near the cloud base. They dominate in the growing and mature phases of cumulus clouds (Paluch and Knight 1984). Entrainment processes and water loading reduce updraft strength, while latent heating (e.g., Zipser 2003) and precipitation (e.g. Fierro et al. 2009; Heymsfield et al. 2010) enhance the updraft strength. In contrast, downdrafts commonly occur in the mature and decaying phases of cumulus clouds. Mature phase downdrafts are generally forced by cloud edge evaporation cooling, which typically occur in the middle level (5–10 km), and entrainment processes near cloud tops. Decay phase downdrafts are forced by precipitation loading, evaporation and melting, occurring below the FZL (May and Rajopadhyaya 1999).

In General Circulation Models (GCMs) convection cannot be represented by modelling individual convective clouds. Instead, simple representations of the collective effects of a cumulus cloud ensemble existing within a model grid-box are applied. Amongst the most widespread of these cumulus parameterization approaches is the so-called mass-flux approach (see Arakawa (2004) for an overview). Here, the vertical transport by the cloud ensemble is directly related to the mass-flux through the clouds, itself a product of the air density, fractional area covered by and the vertical velocity within cumulus updrafts and downdrafts. While conceptually simple, the evaluation of mass-flux approaches from observations has proven difficult, as measurements of the area fraction and vertical velocities within up- and downdrafts on the scale of a GCM grid-box are difficult to ascertain. As a result, much of the evaluation of mass-flux schemes has relied on the use of Cloud Resolving Models (e.g., Randall et al. 2003; Derbyshire et al. 2004; Petch et al. 2014).

The main motivation of this study is to begin closing this obvious observational gap and to demonstrate the potential of using existing observational data set for evaluating model mass-flux schemes. In particular, we wish to address the following two questions: 1) What is the observed vertical structure of convective mass-flux and which of its components (area or velocity) dominates the overall structure? 2) How sensitive is mass-flux to changes in the environmental conditions?

There are previous observational studies that determined direct in-cloud mass-fluxes. Numerous in situ aircraft penetrations conventionally provide the best insights in convective cloud dynamics (e.g. Byers and Braham 1949; Marwitz 1973; LeMone and Zipser 1980; Jorgensen and LeMone 1989; Anderson et al. 2005). However, to facilitate evaluation of mass-flux schemes in GCM, longer temporal length of continuous convective profiling are needed, such as those from advanced remote sensing techniques. Examples of long-term in-cloud mass-flux observations include the works of May and Rajopadhyaya (1999) and Giangrande et al. (2013), where they used wind profiler retrievals from a tropical and subtropical site, respectively. Both studies found the peaks in updraft speeds and updraft core widths associated with deep convection occurred in upper levels, near 10 km altitude. In contrast, downdrafts peaked near the cloud base. In the tropics, updraft cores have smaller speeds, but are wider compared to the subtropics. Heymsfield et al. (2010), who investigated deep convection in both tropics and subtropics using airborne Doppler radars, also reported similar characteristics in vertical velocities for updrafts and downdrafts.

To extract mass-flux over a GCM size grid, we need direct measurements of vertical velocity inside every cumulus clouds enclosed by the model grid box. Most commonly, this is achieved using a dual Doppler radar retrieval technique (e.g. Collis et al. 2013). However, the dual Doppler approach requires at least two radars, with the accuracy of retrieved vertical velocity depending on the location within the radar domain. An alternative and more direct approach to determine vertical velocity is to use wind-profiler (May and Rajopadhyaya 1999; Williams, 2012). The current study will be using the latter approach using data collected in Darwin, Australia, for the two wet seasons (Nov-Apr) of 2005/2006 and 2006/2007. The main difficulty in using wind-profiler observations is that they represent a single atmospheric column and temporal aggregation is required to represent larger spatial areas. By comparing the wind-profiler cloud occurrence with volumetric radar data, we demonstrate that the statistical aggregation of the single column profiler measurements over a longer period do depict convection comparable to that which will be observed in a GCM size grid box. We then proceed to determine both the fractional area and in-cloud velocities in convective up- and downdrafts using the profiler information and aggregate them into GCM-equivalent mass-flux profiles.

Having determined profile of mass-flux from observations over a GCM size box, we evaluate the sensitivity of the vertical structure and strength of the mass-flux to environmental conditions (lower-troposphere (0–5 km) moisture, CAPE and CIN) and the large-scale vertical motion. The Darwin wet season experiences a wide variety of convective systems due to the presence of two distinct convective regimes - active monsoon/oceanic conditions and build-up/break continental conditions (e.g., McBride and Frank 1999; Pope et al. 2009; Kumar et al. 2013b). This makes Darwin a good location to investigate the sensitivity of mass-flux to varying environmental conditions.

Past studies have attempted similar sensitivity tests of mass-flux profiles (or the input parameters used to compute mass-flux) to the synoptic regimes and environmental conditions using both observations and simulations. Cifelli and Rutledge (1994; 1998) using wind profiler observed vertical velocity statistics found significant differences in the mean vertical motion between Darwin break and monsoon storms, with evidence of a bimodal peak in the vertical velocity profile for break cases, while the monsoon cases had a more uniform profile. Here we will extend this study to more details in the environmental conditions. In particular, we will investigate the sensitivity of observed mass-flux to mid- and upper-tropospheric humidity and qualitatively compare the results to those of the idealized CRM simulations in Derbyshire et al. (2004). These simulations implied that in a dry environment, the mass-flux decreases monotonically with height above the cloud base leading to the formation of mostly shallow convection. Moist environments on the other hand led to deep convection with the peak mass-flux located at an elevated height in the mid-troposphere.

The paper is structured as follows. Section 2 will introduce the data sets used in the study. Section 3 describes the method to retrieve velocity and area profiles from wind profiler observations and establishes that these point observations when averaged in time provide a good proxy for mass-flux in a GCM-size grid-box. Section 4 presents the main results of the study, including the mean mass-flux profile and its variability, its sensitivity to environmental conditions, and the contributions from different cloud types to the overall mass-flux. This is followed by a summary and discussion in Section 5.

2. Data

The main goal of this study is to provide observational estimates of convective mass-flux and its components at a scale relevant to the parameterisation of convection in GCMs as well as its sensitivity to environmental conditions. This requires the use of a variety of data sets. Specifically, we make use of a pair of wind-profilers embedded in the field-of-view of a scanning C-band dual-polarization radar and combine those with detailed estimates of the large-scale conditions provided by a variational analysis algorithm. Each of these data sources is explained in turn below.

2.1 The Darwin wind profiler radar pair

We use data collected by a 50- and 920-MHz wind profiler pair from two wet seasons (October 2005 – April 2006 and October 2006 – April 2007), recorded at 1-min resolution. The main advantage of the use of this data source is that wind profilers provide more accurate estimates of in-cloud vertical velocity than other remote-sensing techniques, including Dual-Doppler radar techniques (e.g., Collis et al. 2013). The disadvantage is that the measurements are taken at a single point, but frequently in time, and a time-space conversion is required to make them useful to study the mass-flux behaviour on scales of a GCM grid-box.

Here, vertical velocities are computed by applying the dual-frequency algorithm developed in Williams (2012) to the Doppler returns from the vertical beams of 50- and 920-MHz wind profiler pair. The beam width of the vertical beam is approximately 0.2 km at 1 km height and increases to 2 km by 10 km height. The wind profiler pair was synchronized to begin their vertical beam observations every 1 min. The full description of the Darwin wind profiler setting can be found in Williams (2012).

The 50-MHz profiler simultaneously observes both Bragg scatter from ambient air, which provides a direct measurement of the vertical velocity of air parcels (wanted signal), and Rayleigh scatter from hydrometeors (unwanted signal). If signals from the two scattering processing are not properly separated, then the vertical air motion estimates will be biased downwards because of contamination from falling hydrometeors. The Williams (2012) method uses the spectra from the 920-MHz profiler, which are sensitive to mainly hydrometeor returns, to filter out the Rayleigh echo returns from the 50-MHz profiler spectra. The filtered 50-MHz signal is then processed using the standard wind profiling processing technique described in Carter et al. (1995) and is based on the profiler online processing (POP) routine. The POP routine estimates the spectrum noise level, the spectrum signal start and end integration points, and the first three moments—power, mean reflectivity-weighted Doppler velocity, and the spectrum width (equal to twice the spectrum standard deviation). The mean Doppler velocity corresponds to the vertical air motion. The accuracy of the vertical velocity retrieval by the Darwin wind profiler pair is estimated to be between 0.05 to 0.25 m s^{-1} using a Monte Carlo simulation design (Williams 2012). Further comparisons between the Darwin wind profiler and statistical techniques for the separation of terminal fall velocity and vertical air velocity also yielded an agreement to within 0.1-0.15 ms^{-1} (Protat and Williams 2011).

The profiler vertical velocity measurements are interpolated onto a vertical grid of 100 m resolution over an altitude range of 1.7 – 17 km. However, the highest quality data is thought to be limited to heights below 11 km (May and Rajopadhyaya 1999), because of the reduction in profiler sensitivity with height.

Finally, the vertical velocity data from the wind profiler was further filtered to keep only measurements that were from within cumulus clouds (see Section 3 form more detail). To achieve this, we need to know; i) if a cumulus cloud occurred at the profiler site, and ii) what the estimated cloud top height of the cumulus cloud at the time of the profiler measurement might be. This information on the physical properties of the clouds is extracted from the collocated C-band scanning radar, which contains the wind profilers within its field-of-view, roughly 24 km southwest from the radar location (see Fig. 1 of May et al. 2002). The CPOL measurements are introduced in more detail in the following subsection. Vertical velocities outside cumulus clouds are not considered here.

2.2 Darwin CPOL radar

We use measurements of reflectivity from the C-band polarimetric radar (CPOL; Keenan et al. (1998)), which have been sampled onto a cubic grid with a horizontal grid size of 2.5 km x 2.5 km, and vertical resolution of 0.5 km. The horizontal scanning area of CPOL is approximately 70,000 km^2, sufficient enough to contain few GCM size grid boxes.

The CPOL measurements are used to identify different cloud types that are present over the wind profiler. Here we make use of earlier studies (e.g., Kumar et al. 2013a-b; 2014) that demonstrated the utility of the CPOL measurements to identify convective cloud cells and determine their cloud top height. We make use specifically of two physical characteristic derived from the CPOL data in this study:

i) We apply a convective vs stratiform classification and use only those clouds identified as convective over the wind profiler to extract their mass-flux characteristics.

Specifically we apply the widely used Steiner algorithm to identify convective clouds (Steiner et al. 1995) at the CPOL pixel collocated with the wind profiler location. This algorithm has been successfully employed in several previous studies to differentiate between the convective and stratiform cloud types (e.g. Kumar et al. 2013a-b; Penide et al. 2013a). As the CPOL radar takes 10 minutes to complete a full volume scan, all 1-min scans of the wind profiler falling into a 10-minute interval of convective cloud occurrence over the profilers are used as valid measurements of vertical velocity.

ii) As our focus is on convective mass-flux, we would like to filter out any vertical velocity measurements taken in cirrus anvils and/or in clear air above active convective drafts. To do so we make use of the 0-dBZ echo top height extracted from the CPOL reflectivity profile over the profiler site. Previous studies have shown that the 0-dBZ echo tops from C-band radar observations are usually within 1 km of cloud top heights estimated by millimetre cloud radars such as that on CloudSat (Casey et al. 2012) or on the ground at Darwin (Kumar et al. 2013a). To ensure that we study continuous up- or downdrafts we require that there is vertically continuous reflectivity signal between the lowest CPOL level of 2.5 km height and the 0-dBZ echo top. We also apply the echo top height to classify the observed cumulus clouds as either congestus, deep and overshooting (Kumar et al. 2013a; 2014), allowing us to investigate the contribution to total mass-flux from the various cumulus modes.

2.3 Background environmental conditions

Apart from providing overall mass-flux estimates we also aim to examine the effects of the environmental conditions on the mass-flux behaviour. To do so requires reliable observational estimates of key environmental parameters. Here we use 6-hourly information on lower-troposphere (0–5) km relative humidity (RH_{0-5}), CAPE (Convective Available

Potential Energy), CIN (Convective inhibition), and the large-scale vertical motion at 500 hPa (ω_{500}). We use two main sources to derive these parameters.

The $RH_{0\text{-}5}$ is extracted from the Darwin airport operational radiosoundings. We simply average the relative humidity measurements between 0 and 5 km. The remaining three parameters, CAPE, CIN and ω_{500}, were from a large-scale data set derived for the Darwin region by Davies et al. (2013) by applying the variational budget analysis technique of Zhang and Lin (1997) using NWP analysis data as "pseudo-radiosondes" and radar and satellite observations at the surface and top of the atmosphere, as suggested by Xie et al. (2004). By comparing their approach to results from the Tropical Warm Pool International Cloud Experiment field study (May et al. 2008), Davies et al. (2013) showed that this technique provides much better estimates of the large-scale state of the atmosphere than the direct use of analyses or reanalyses from Numerical Weather Prediction Centres. The median over the two wet seasons for CAPE, CIN, ω_{500}, respectively, were 548 J kg^{-1}, 43 J kg^{-1} and −0.38 hPa Hour^{-1}. Note that a negative value for vertical motion represents upward motions.

3.0 Method

The main motivation of this study is to provide a statistical picture of mass-flux profiles using observations, which will then be useful to evaluate existing cumulus mass-flux scheme in models and assess the respective contributions of convective area fraction and vertical velocity to updraft mass flux. Ideally, this would require high resolution observations of vertical velocity both in time and space over a volume of 100 km x 100 km in the horizontal (typical GCM grid box) and 20 km in the vertical. No such measurements exist. As outlined in the introduction, in this study we will make use of vertical velocity retrievals as derived from dual-frequency wind profiler observations. However, we will combine the wind profiler information with that from the scanning CPOL radar to investigate the representativeness of the single site measurements for convection over a GCM size grid.

While our overall goal is to provide a statistical study of several hundred cumulus cells occurring over time in a GCM box we first illustrate our methodology to derive vertical motion and area fraction profiles using a snapshot of a deep convective case observed concurrently by both radar types shown in Figure 1. Figure 1a shows the time-height cross-section of reflectivity from the CPOL radar at the profiler site, which is available in 10 min time intervals and 0.5 km resolution in height. The remaining panels of Fig. 1 show the wind profiler measurements. The profiler observations are available at a much finer resolution of 1 min in time and 0.1 km in height. The red circles in Fig. 1a depict the 0-dBz ETH locations at those times where the Steiner classification finds a convective cloud over the profiler site (also indicated by the black line).

The differences between the CPOL reflectivities (Fig. 1a) and the 50 MHz (Fig. 1b) and 920 MHz (Fig. 1c) wind profiler reflectivities are found to be quite large, with the CPOL reflectivities in better agreement with the 920 MHz wind profiler reflectivities than with the 50 MHz wind profiler reflectivities. This is not surprising, as the 50 MHz wind profiler reflectivities are a mixture of echoes from clear air and hydrometeors, while CPOL is only sensitive to hydrometeors. The differences between CPOL and the 920 MHz reflectivities likely reflect the high temporal evolution of the convective event within the sampling resolution of CPOL (10 minutes), which is captured by the 920 MHz observations at 1-minute resolution.

Examinations of CPOL radar loops for the event described in Fig. 1 revealed that the overshooting convective system sampled in Figure 1 was embedded in widespread stratiform clouds and the whole system was moving across the profiler from the southwest. The time-height sections of vertical velocity (Fig. 1d) indicate that the storm was present over the profiler location for approximately one hour. The regions with vertical motion exceeding 1.5 m s^{-1} (strong updrafts) and below −1.5 m s^{-1} (strong downdrafts) are shown by the black contours. The upward motions first occur at the low-levels around 0440 LT, coinciding with the arrival of the storm. Within 30 min the region of strong upward motion shifted rapidly from low-levels to above the freezing level (approximately 5 km). From between 0520–0540 LT, the updrafts remain constantly strong between 5 and 15 km. After 0550 LT, there is a secondary increase in upward motions at around 7 km. By this time, the main convective cell had passed over the profiler sites and the profiler is now sampling the stratiform anvils of the storm as indicated by the absence of convective clouds in Steiner classification applied to CPOL (Fig 1a).

While present in Figure 1 it is evident that downdrafts occur much less frequently and with much weaker magnitudes than updrafts. This is well known and has been illustrated in other studies using radar profiler measurements (e.g. see May et al. 2002; Heymsfield et al. 2010; Giangrande et al. 2013). The observed regions of downdrafts, although short-lived (so smaller spatial width), are consistent with the different downdraft types known to exist (e.g., Knupp and Cotton 1985). Downdrafts forming at low levels, which are more frequent than downdrafts in higher levels, are likely associated with precipitation loading, evaporation and melting and can be seen throughout the active storm phase. Several downdrafts can be found at mid levels, such as the observed strongest downdraft around 0540 LT between 7 and 10 km. They are thought to be forced by cloud edge evaporation cooling. Note that we frequently observe downdrafts in the stratiform regions of the cloud system sampled in our data set. As we focus on convective situations only, these will not form part of our analysis. Downdrafts are also observed between 10 and 15 km near the cloud tops. These are thought to be penetrative downdrafts, which are short-lived (i.e., of small size) and are likely the result of the entrainment of sub-saturated air into the cloud. It is clear from the case study illustrated in Figure 1 that vertical motions vary significantly over the storm lifetime, height and also between convective and stratiform structures. We do not attempt to study the evolution of vertical velocities as function of storm lifetime because the profiler may be sampling only a section of individual storms.

To be of use for model evaluation, the derived mass-flux profiles must be representative for an area the size of a GCM grid-box. To account for all cumulus clouds over the model size grid requires computation of convective area fraction. The area fraction is typically defined as the ratio of the size of all convective cells in the domain over the total domain size. Scanning radars, such as CPOL, are the most suitable to calculate area fraction using this spatially sampling approach. Since we wish to compute mass-flux from a vertically pointing wind profiler, which takes measurements over a column with a small cross-section area, the area fraction cannot be directly estimated using these measurements. . Instead convective area fraction is determined as the ratio of the time CPOL identifies convection above the profiler over the total sampling time. We use a long total sampling time of two wet season with the rationale that the convection, at a point, derived from this long time series is a good sample of that occurring in the entire domain over the same sampling time.

To evaluate this approach, the area fractions were derived as described above using both the scanning CPOL and vertically pointing wind profiler, respectively (Fig. 2). Recall that only convective cloud columns from CPOL are used to calculate both the spatial statistics from CPOL and the temporal statistics at the profiler site. The convective area fraction from CPOL was calculated for various circular regions of radius ranging from 10 to 100 km centered on the wind profiler site. The CPOL area fractions for three selected domain sizes shown in Fig. 2 are remarkably similar. This suggests that convection experienced at the profiler site is a good approximation for convection experienced in a GCM size grid box centered on the wind profiler location. Importantly, the convective area fraction derived from the wind profiler for the whole time period (solid curve, $|v| \geq 0$ m s^{-1}) shows a similar structure as the area fraction from CPOL in the lower and middle troposphere but drops off more rapidly above 8 km. The CPOL radar takes 10 mins to complete each volumetric scan, so when present it is assumed that the convection will last for the entire 10 mins. The example discussed in Fig. 1 shows that the temporal variability is high within 10 minutes, with large differences observed between CPOL and 920 MHz reflectivities. In contrast, the wind profiler samples every 1 min, so even though a 10-min window is classified as convective by CPOL, the individual ten 1-min profiles from the wind profiler does not always contain valid vertical velocity measurements. Inevitable instrumental problems may have further contributed to this. Also, at higher altitude, the profiler area fraction begins to drop relatively rapidly compared to the CPOL fractions due to the drop in profiler sensitivity with altitude. The CPOL sensitivity does not change much with height.

We further evaluate the area fraction estimates from the profiler by applying consecutively larger thresholds to the vertical velocity measurements. The thresholds of $|v|$ greater 0.5, 1.0 and 1.5 m s^{-1} are chosen as they have been employed by previous investigators to identify updraft/downdraft cores in cumulus clouds (e.g., LeMone and Zipser, 1980; May et al. 2002; Giangrande et al. 2013). Changing the velocity threshold leads to significant differences in area fraction from the two radars, in particular below the freezing level. Above the height of 10 km, the fractions for different thresholds are similar because the profiler is detecting only highly reflective regions from the high altitudes. From hereon we will use all vertical velocity data points from the identified convective periods at the profiler without applying any further thresholds since the profiler-derived area fraction with no threshold was closest to the CPOL area fractions and therefore likely captures best the behaviour of the entire domain more robustly.

Equipped with estimates of area fraction and in-cloud vertical velocity from the profiler measurements we can now calculate the mass-flux M_c (kg s^{-1} m^{-2}). Here, M_c is defined using the traditional GCM-type definition for mass-flux by considering all cumulus cloud occurring over a large area:

$$M_c = \rho\sigma_u v_u + \rho\sigma_d v_d \qquad (1)$$

where: ρ is the air density (kg m^{-3});

σ_u , is the area fraction of updraft cores in the grid box and is a dimensionless quantity. The σ_u can be further subdivided into the numbers of cores and the width of cores;

v_u is the mean velocity of updraft (m s^{-1}) ;

and σ_d and v_d is the area fraction and mean velocity of the downdraft cores, respectively.

The vertical profile of air density is computed using standard textbook formulae, with input temperature and pressure fields extracted from the Darwin radiosonde. The mean profiles of all remaining variables in Equation (1) are computed using the profiler vertical velocity data from the convective intervals. We found that unlike the area fraction, the mean mass-flux profile was largely independent of the different velocity threshold (result not shown). This is so since larger vertical velocity thresholds lead to smaller area fraction (Fig. 2) but much larger mean vertical velocities with the two effects compensating and leading to similar mean mass-flux values.

4. Results

4.1 Overall characteristics of convective mass-flux and its components

a) Mean mass-flux profile

Convective clouds were identified by the CPOL radar over the profiler site for a total of 283 10-minute scans during the two wet-seasons analysed here. This corresponds to a convective area fraction near the surface of approximately 0.5 %. Note that this represents an average including many instances with no convection present in the domain for significant periods of time. It is therefore not comparable to convective area fractions found in previous studies (e.g., Davies et al. 2013), which reach values up to 10 % but reflect instantaneous conditions rather than long temporal averages. Going back to the overall time average, Table 1 summaries the contributions to the total convective area fraction from congestus (CTH < 7 km), deep (CTH between 7 and 15 km) and overshooting clouds (CTH> 15). It also shows the variability of convective cloud frequency as function of different environment and large-scale terciles. The results shown in Table 1 are discussed further in sections 4.2 and 4.3.

Mean profiles of the overall mass-flux as well as upward and downward mass-flux profiles are shown in Fig. 3. Here, the lower x-axis represents the overall mean over the entire two seasons including the very frequent times (99.5%) of no convective clouds present over the profiler site. To provide at least a rough estimate of the values of mass-flux “when present”, a value more useful to modellers, we average mass-fluxes over 3-hour windows and discard all windows with no presence of convective clouds (~93 %). The results are indicated by the upper x-axis in Figure 3. A 3-hour window translates to a grid size of roughly 60 km; calculations based on 5 m s^{-1} mean average propagating speed of convective cells [Kumar et al. 2013b]. Note that removing zeros will not affect the profile shape but only its magnitude.

The overall mean mass-flux (thick curve) increases steadily from near cloud base to peak at 6 km just above the freezing level, and thereafter decreases gradually with height. At all levels, except at very high altitudes, the mass-flux totals are dominated by updrafts (thin curve). Importantly, these observational results also validate those reported in many studies using cloud-resolving models (e.g. Derbyshire et al. 2004; Kuang and Bretherton, 2006) and are also in good agreement with previous attempts to retrieve mass-fluxes from profiler observations (e.g., May and Rajopadhyaya, 1999).

b) Mean area fraction and vertical velocity

Equation 1 indicates that updraft and downdraft mass-fluxes are affected by three fundamental factors; the number of cores, the size of the cores and the vertical velocity in the cores. The product of the number and size terms divided by domain size gives the area fraction. We now examine the characteristics of these three fundamental factors with the aim to understand the relative contributions of these factors to the mass-flux totals.

We begin by examining the variations in convective area fraction (thick solid line in Fig. 4a) divided into upward area fraction (thin solid line) and downward area fraction (dashed line). Once again we show the overall period averages with the lower x-axis and those for 3-hour windows that contain convection with the upper x-axis. At low levels, updraft and downdraft area fractions are nearly equal. The updraft fraction remains more or less constant from near the surface to 8 kilometre and then decreases steadily at higher levels. Starting from the top the small downdraft fraction increases slightly to just above the freezing level, where a significant increase in downdraft fraction occurs, indicating the potential importance of this level in downdraft formation. In Fig. 4c and 4d, the upward and downward area fractions (shaded) are subdivided into the number of cores (solid lines) and their size (dashed line). The core width is measured in minutes, and represents the number of consecutive 1-min periods with vertical motion $>0\,\text{m s}^{-1}$ for an updraft core. Downdraft cores are defined analogously using downward motion.

The mean core width associated with upward motion (dashed line in Fig. 4c) increases gradually from an average of ~2 min at cloud base to a maximum average width of ~6 min at a height of 8 km. Assuming a propagation speed of 5 ms^{-1}, this translates into a width of ~600 m near cloud base and ~1.8 km at mid-levels. Above 8km the updraft core width decreases sharply. In contrast, the core frequency associated with updrafts is highest near cloud base, decreasing monotonically with increasing height. The net effect of this pattern in updraft width and frequency is that the upward area fraction is highest and constant between cloud base and 8 km. Downdraft number increases downwards with a particularly sharp increase near the freezing level. The average width of downdraft cores is ~3 min and remains fairly constant with height. Once again assuming a 5 ms^{-1} propagation speed, this translates into a size of ~900 m.

The mean vertical velocity (thick curve in Fig. 4b) increases gradually with height and peaks at ~4 m s^{-1} at 12 km. The mean profile of vertical velocity is the sum of the velocity in updrafts (thin curve in Fig. 4b) and downdrafts (dashed curve) weighted by the fractional area of up- and downdraft cores. The updraft velocity evolution with height is very similar to the mean with a drop between 2 and 3 km followed by a steady increase to values of ~5 m s^{-1} at high levels. In contrasts, the downdrafts show much weaker velocities of ~ 1 m s^{-1} which are almost constant throughout the cloud layer with slightly large values near the tops of very deep clouds.

Next, we reconcile the vertical structure of the mass-flux (Fig. 3) with area fraction (Fig. 4a, Fig.4c–4d) and vertical velocity (Fig. 4b). As it is difficult to mentally sum all contributing factors to the total mass-flux we compare the updraft and downdraft terms separately. The increase in updraft mass-flux between 2 and 5 km is largely a reflection of the vertical velocity increase combined with a small increase in area fraction. The large reduction in updraft mass-flux above 8 km is due to the strong decrease in area fraction, which is slightly offset by an increase in vertical velocity. Note that the decrease in density with height also affects the overall mass-flux profile so that constant velocity and area fraction would still imply a reduction of mass-flux with height. As the downdraft velocities are small and relatively constant with height, the strong increase in downdraft mass-flux below 6 km (Fig. 3) is to first order driven by the corresponding increase in downdraft area fraction.

Overall, perhaps with the exception of the low-level increase of updraft mass-flux, the total mass-flux is governed to first order by the area fraction. If confirmed at other locations, this would provide the opportunity of estimating the first order characteristics of mass-flux from area fraction alone, a quantity that is much more easily measured using instruments both on the ground and in space than vertical motion.

4.2 Sensitivity of mass-flux to environmental and large-scale conditions

Of key relevance to cumulus parameterisation is the connection of mass-flux with the environmental conditions in which the convection is embedded. In this section, we examine the relationship between $RH_{0\text{-}5}$, CAPE, CIN and ω_{500} with the updraft mass-flux, upward area fraction and upward velocity. As the downdraft contribution to overall mass-flux is relatively small we focus on updraft behaviour only.

For the analysis shown in this section, the environmental conditions are grouped into terciles of their respective probability density functions. This ensures that the wind profiler sampling time in each tercile is identical. Note though that the amount of convective clouds observed in each tercile can still vary significantly depending on how favourable the conditions in each tercile are for convection. The tercile boundaries for each variable, the amount of time with which convective clouds occur in each tercile and their sub-division into congestus, deep and overshooting modes are shown in Table 1.

a) Effect of 0-5 km Relative Humidity (RH_{0-5})

A moist environment, which is represented by the upper tercile of RH_{0-5}, is thought to be important to support the formation of deep convection over its shallower counterparts (e.g., Redelsperger et al. 2002; Takemi and Liu 2004). The results shown in top panels of Fig. 5 reveal several interesting differences between dry (solid curves, RH_{0-5}<68%) and moist (dashed curve, RH_{0-5}>82 %) conditions updraft mass-flux (left), area fraction (middle) and velocity (right). The updraft mass-flux (Fig. 5a) in dry conditions exhibits a sharp peak at the height of 6 km with a strong drop-off in mass-flux above that level, while in moist conditions a smoother and deeper mass-flux profile is evident. The behaviour in dry conditions likely indicates the prevalence of shallower clouds (see Section 4.3). The updraft area fraction is much smaller in dry conditions, indicative of a less frequent occurrence of convection (see also Table 1). As seen before for the overall means (Fig. 3 and 4), area fraction increases from cloud base to mid-levels, followed by a decrease higher up. Vertical velocity increases with height in both states of RH_{0-5}. Perhaps surprisingly, the velocities are stronger in dry conditions than in moist conditions, partly compensating the lower mass-flux strength induced by the lower area fractions in that state. The higher velocities can be understood by the need to produce stronger updrafts to penetrate through the dry atmosphere, while in moist conditions weaker updrafts occur more frequently and can penetrate higher into the moist troposphere more easily.

b) Effect of CAPE

We next study the relationship of mass-flux to CAPE (Fig. 5d–f). The differences in the upper (> 747 J kg^{-1}; dashed) and lower tercile (<365 J kg^{-1}; solid) CAPE conditions are much smaller than those for $RH_{0\text{-}5}$. The mass-flux is slightly weaker in low CAPE conditions and it reaches higher levels in high CAPE conditions. Somewhat paradoxically, low CAPE conditions give rise to higher area factions. This is consistent with the findings of Kumar et al. (2013b) who showed that low CAPE conditions are associated with more frequent but shallower convective clouds over Darwin. The air parcels in the convective clouds are less buoyant in low CAPE conditions, leading to weaker updraft speed (Fig. 5f) and often shallower cloud. In contrast, in high CAPE condition, convection is much deeper because the air parcels have greater growth momentum. While less frequent in high CAPE conditions, convection that occurs does show significantly larger vertical velocity. The net effect is that the updraft mass-flux at all heights, except near cloud base, is higher in high CAPE conditions compared to low CAPE.

c) Effect of CIN

In general, when the convective inhibition (CIN) of the atmosphere is low, more convective cloud systems are likely to form. This is confirmed by our analysis of mass-flux in the lowest (< 30 J kg^{-1}; solid) and highest (> 62 J kg^{-1}; dashed) CIN terciles (Fig. 5g–i). There is a large difference in mass-flux between high and low CIN conditions, which is entirely caused by differences in area fraction, which is synonymous with the frequency of occurrence of convection. The vertical velocity profiles are largely unaffected by the state of CIN, indicating that CIN is more likely a predictor for the existence of convection than its strength.

d) Effect of large-scale upward motion at 500 hPa (ω_{500})

Similar to CIN, large-scale vertical motion is strongly related to the existence of convection (Fig. 5j-l). Almost all convective events occur in the "lower" tercile, which comprises upward motion ($\omega_{500} \leq -1.82$ hPa Hour^{-1}, solid), while the upper tercile of large-scale downward motion ($\omega_{500} \geq 1.24$ hPa Hour^{-1}, dashed) is more or less void of convection. The very small fraction (7%) of convective systems that do form when there is large-scale downward motion tend to have very high vertical velocities in the upper part of the updrafts, although the poor sampling in this class prevents us from drawing any firm conclusions.

e) Summary of effects of environmental conditions on mass-flux

In its entirety Fig. 5 provides an important set of lessons about convective behaviour that can potentially be used in the construction of cumulus parameterisations. It is clear that different environmental parameters, many of which have been used in constructing elements of existing cumulus schemes, have different effects on the mass-flux, mainly because they affect its two components, area and velocity, in different ways. Large-scale vertical motion and CIN are strongly related to area fraction. These conditions strongly influence the existence and prevalence of convection and through the area fraction exerts a strong control on the convective mass-flux. In addition, $RH_{0\text{-}5}$ is also strongly related to vertical motion in the clouds, although it is likely that there is no direct causality in that relationship. Instead, we speculate that the higher velocities in dry conditions are a result of weaker updrafts not being able to penetrate the dry atmosphere. Changes in CAPE have the least impact on the convective area fraction but instead show a strong relationship with cloud growth dynamics. In low CAPE conditions, the convective systems tend to be moderately more frequent but with weak updraft speed while high CAPE conditions support stronger vertical motion, leading to overall slightly higher mass-fluxes in those conditions. In summary, there is some evidence from Fig. 5, that the components of mass-flux are responding differently to different environmental conditions, making it difficult to relate mass-flux itself to only one of them. This may indicate a potential benefit from treating area and velocity separately in future cumulus parameterisation approaches.

4.3 Contributions of each cumulus cloud type to the total mass-flux in different environmental conditions

Having investigated the overall mass-flux properties and their relationship to the state of the environment the convection is embedded in we now investigate the contributions of individual cumulus cloud modes, namely congestus, deep and overshooting clouds, to the overall cumulus mass-flux. The three cloud modes are defined by tracking convective cells and identifying their maximum echo top height (ETH, Kumar et al. 2013a, 2014). Cells that never exceed a 7 km ETH are classified as congestus, those that exceed 15 km ETH are classified as overshooting and the rest as deep convection. Kumar et al. (2013a) noted that these three modes have remarkably different rainfall and drop size characteristics, and thus, it will be worthwhile to examine the vertical velocity and mass-flux characteristics of these cumulus modes separately as well as quantify their overall effect.

The breakdown of the total time for which the three cumulus convective modes are found at the profiler site is shown in Table 1. We find that the most frequent type of convection sampled by the profilers is deep convection, with just over half of all cases in this category. The other two types contribute roughly one quarter each to the overall sample.

The mean profile of upward mass-flux associated with the three cumulus modes and the components of these mass-flux profiles are displayed in Fig. 6. Given its high frequency the highest contribution to the upward mass-flux in the lower 8 km of the troposphere is from the deep mode. The mean vertical velocity intensity of this mode shows intermediate strength updraft velocities of 2 to 4 m s^{-1} with a bimodal structure with peaks at 6 km and above 10 km. The congestus mode contributes about one quarter of the area fraction below 4 km, but due to its relatively weak upward motion on the order of only 1 m s^{-1} makes a relatively small contribution to overall mass-flux. The overshooting mode contributes around one quarter to the area fraction below 10 km and dominates the area fraction above that level. It shows the strongest vertical motion of the three modes with average values increasing from around 4 m s^{-1} at 5 km to 6 m s^{-1} above 10 km.

As the mass-fluxes were shown to be sensitive to the environmental conditions we next investigate how the relative contribution from the three cloud modes may change with the state of the environment. It was evident from Fig. 5 that ω_{500} and CIN mostly determined the existence of convection, while RH_{0-5} and CAPE had a more direct influence on its structure. We therefore focus on the latter two parameters.

The total time of each cumulus mode during the different environmental conditions are given in Table 1. The most notable change in total time of individual cumulus modes with respect to different environment conditions occurs for the overshooting mode when sorted with respect to CAPE. While constant in overall terms (Fig. 7h and k), overshooting cloud forms 17% of all convection in low CAPE conditions but 37% in high CAPE conditions. This is a result of the occurrence of both the congestus and deep mode decreasing as CAPE increases (Fig. 7 h and k). As expected, the vertical velocities for the deep and in particular for the overshooting mode increase with CAPE (Fig. 7i and l), leading to the overall larger mass-fluxes in high CAPE conditions discussed earlier (Fig. 5). We now see that this increase is predominantly driven by an increase in the velocities in the overshooting mode.

Changes in RH_{0-5} (Fig. 7a–f) also strongly affect the overall mix of the occurrence of convective modes. In dry conditions, 60% of the time convection is present is associated with either the congestus or overshooting mode. In contrast, in moist conditions the deep mode becomes the dominant mode occurring 54% of time. The area of all three convective modes increases significantly in moist conditions (Fig. 7b and e), while the velocities in the deep modes decrease by about half with little change in the congestus mode. This once again highlights that deep convection of both types is stronger but less frequent in dry conditions.

4.4 Variability in mass-flux measurements

The results shown so far have focused entirely on the mean behaviour of mass-flux and its components, although some indication of variability is revealed by the breakdown into cloud modes. In this section we aim to investigate the variability of mass-flux at the typical scale of a GCM grid box across different events, as this is more readily comparable to what the mass flux parameterization produces. To enable this investigation we need to compute the mass-flux over some discrete time window rather than averaging over long periods of time. This once again requires finding a compromise between representing the size of a GCM grid-box and the results being affected by the time evolution of the convective systems over the time window. We choose a 3-hour time averaging window (~60 km), but we will also contrast our results to those found using a longer, 6-hour, window (~100 km). As most time-windows will have no convection at all in them, we focus our investigation on the 95th, 99th and 99.5th percentile of the respective distribution functions. Figure 8 shows these percentiles for area fraction (top) and mass-flux (bottom) for both the 3-hour (green) and 6-hour (red) time windows. For comparison, we include the area fractions measured by CPOL in a 50km radius around the profiler site in Figure 8a.

While the length of the time window does not affect the mean profile of area fractions, it does affect the variability. Shorter time windows will produce larger variability because there will be increases in incidence of both very large and very small area fraction. Of the 2300 (1150) available 3-hour (6-hour) time blocks 93% (88%) had a convective area fraction of 0. As expected, the upper percentiles of the area fraction distribution yields larger (smaller) values for the 3-hour (6-hour) window ranging from 0.05 (0.03) for the 95^{th} percentile to 0.1 (0.08) for the 99^{th} percentile. The 6-hour window is in closer agreement with the CPOL area fractions.

The upper percentiles of the mass-flux distribution associated with the 3- and 6-hour windows are shown in Fig. 8b. This figure is in the same format as Fig. 8a, except the 98^{th}, not the 95^{th} percentile is shown, as the 95^{th} percentile mass-fluxes were too small to be seen clearly. The 98^{th} percentile mass-fluxes have the same shape as the mean updraft and downdraft mass-flux profile (Fig. 3), with peak updraft and downdraft mass-flux just above the freezing level and close to cloud base, respectively. At higher percentiles very large updraft mass-flux values can be seen at higher altitude and are associated with large vertical velocity events associated with deep and overshooting convection.

5. Summary and Discussion

The aim of this study was to derive convective mass-fluxes and their components on the scale of a GCM grid-box from wind-profiler observations and thereby to provide a zeroth-order observational reference for the evaluation of cumulus mass-flux schemes. The analysis conducted characterised the updrafts and downdrafts of convective clouds with continuous dual-frequency wind profiler observations taken over two wet-seasons near Darwin, Australia. We found the net mass-flux over the entire measurement period to be positive (upwards) between 2 and 14 km height with a peak at ~6 km. The downdraft cumulus mass-flux was shown to be strongest close to cloud base associated with precipitation processes, with vertical motion values of less than half of that seen with the updrafts.

The separation of mass-flux into velocity and area fraction, the latter itself a product of core width and frequency, showed that the mass-flux was most strongly regulated by area fraction compared to the vertical velocity. While of secondary importance to overall mass-flux magnitude, the vertical velocity intensities revealed some crucial properties related to the cloud dynamics. The convective updraft velocity exhibited a dominant peak in the upper-levels (>10 km), and a small secondary peak in lower level at 6 km particularly associated with the deep convective cloud mode. The observed structures in vertical velocity intensities associated with the deep convection (Fig. 6) matched well with the updraft profiles reported in Heymsfield et al (2010). The overshooting convective mode had more intense vertical velocity magnitudes than the deep mode at all height levels, increasing monotonically with height.

By separating the mass-flux into contributions from different cloud types, we demonstrated that wide variety of vertical velocity intensities and cumulus sizes contribute to the mean mass-flux profile. This was shown to be due to a complex interplay of the frequency, size and strength of cumulus clouds with the environment. The analysis revealed that ~80% of the cumulus population over the two seasons formed when the large-scale vertical motions were strongly upwards (≤ -1.82 hPa Hour^{-1}) and/or when CIN was small (≤ 30 J kg^{-1}). Both low-level relative humidity (RH_{0-5}) and CAPE had a more moderate effect on the existence of cumulus clouds but these parameters had a significant impact on the vertical velocity and hence growth dynamics of the clouds. Higher mean velocities were mainly associated with deeper convection that formed in dry ($RH_{0-5} < 68\%$) and high CAPE conditions (Fig. 5 and Fig. 7). While the latter is easily explained by energetic arguments, the former is a less obvious result. We interpret this result as driven by the effects of the entrainment of dry air into the clouds limiting the vertical growth of clouds (e.g., Redelsperger et al. 2002). The very few deep cumulus clouds that do succeed to grow in unfavourable dry conditions need very strong vertical growth momentum and hence display very large vertical velocities.

The downdraft vertical velocities and frequencies were significantly less than those for updrafts at all height levels, except at cloud base and near cloud top, where they were similar. This is consistent with the conceptual picture that a convective cloud is generally made up of one or more dominant updraft cores, which are partly compensated by small and short-lived downdrafts driven by evaporative cooling from both cloud and precipitation hydrometeors (see Fig 1).

Our study has extended previous investigations, such as studies of May and Rajopadhyaya (1999) for the tropical Darwin region and Giangrande et al. (2013) for mid-latitude central plain of United States by examining not only the overall mass-flux but its components at scales relevant to GCM evaluation. Unlike these studies, we accepted all values of vertical motion in our statistical analysis rather than setting a threshold value. This led to better agreement with convective area fraction profile shapes derived from the CPOL scanning radar (Fig 2), likely making our sample more representative. The mean updraft and downdraft vertical velocity profiles found here are nevertheless in good agreement with earlier studies (e.g., Heymsfield et al. 2010). The sensitivity of mass-flux to the environmental moisture conditions is in broad agreement with the modelling study of Derbyshire et al. (2004). Both the observational and model results show that during the moist conditions, the mass-flux has a broad peak at mid levels, while in dry conditions, the mass-flux decreases monotonically with height albeit this decrease starts at higher levels in the observations (4 km) than in the model simulations (cloud base).

Despite the availability of two wet seasons of observations, perhaps the biggest limitation of our study remains the relatively small sample size. This once again highlights the difficulty of supporting the development of cumulus parameterizations with the relevant measurements. An obvious way to alleviate this problem is to use data from scanning radar systems. Such systems can provide frequent measurements of convective area fractions at GCM grid-box scale (e.g., Davies et al. 2013) but the challenge is to derive long time series of reliable retrievals of in-cloud vertical velocity from them. This will be the next step of this work. We will use the computationally-efficient dual-Doppler retrieval technique from Protat and Zawadzki (1999), which will be evaluated first using the wind profiler vertical velocities as in Collis et al. (2013), but applied to a much longer dataset over Darwin. Our finding that mass-flux profiles tend to be dominated by the convective area fraction and that in-cloud velocities vary with cloud depth may also enable us to derive mass-flux estimates from scanning systems by statistically modelling, rather than measuring, vertical motion and combining those with more easily observed area fractions. This will be the subject of a further study that will extend the first useful foray into supporting cumulus parameterization development more directly with long-term observations presented in this paper.

References

Anderson, N. F., C. A. Grainger, and J. L. Stith, 2005: Characteristics of strong updrafts in precipitation systems over the central tropical Pacific Ocean and in the Amazon. *J. Appl. Meteor.*, 44, 731–738.

Arakawa, A., 2004: The Cumulus Parameterization Problem: Past, Present, and Future. *J. of Climate*, **17**, 2493–2525.

Byers, H. R., and R. R. Braham, 1949: The Thunderstorm—Report of the Thunderstorm Project. U.S. Weather Bureau, 287 pp.

Casey, S. P. F., E. J. Fetzer, and B. H. Kahn, 2012: Revised identification of tropical oceanic cumulus congestus as viewed by CloudSat. *Atmos. Chem. Phys*., **12**, 1587–1595.

Carter, D. A.,K. S.Gage,W. L. Ecklund, W. M. Angevine, P. E. Johnston, A. C. Riddle, J. Wilson, and C. R. Williams, 1995: Developments in UHF lower tropospheric wind profiling at NOAA's Aeronomy Laboratory. *Radio Sci.*, 30, 977–1001.

Cifelli, R., and S. A. Rutledge, 1994: Vertical motion structure in Maritime Continent mesoscale convective systems: Results from a 50-MHz profiler. *J. Atmos. Sci.*, **51,** 2631–2652.

Cifelli, R., and S. A. Rutledge, 1998: Vertical motion, diabetic heating, and rainfall characteristics in N. Australia convective systems. *Quart. J. Roy. Meteor. Soc.*, **124,** 1133–1162.

Collis, S., A. Protat, P. T. May, and C. Williams, 2013: Statistics of storm updraft velocities from TWP-ICE including verification with profiling measurements, *J. Appl. Meteorol. Climatol.*, *52*, 1909–1922.

Davies, L., C. Jakob, P. T. May, V. V. Kumar, and S. Xie, 2013: Relationships between the large-scale atmosphere and the small-scale state for Darwin, Australia. *J. Geophys.* Res., DOI: 10.1002/jgrd.50645.

Derbyshire, S. H., I. Beau, P. Bechtold, J.-Y. Grandpeix, J.-M. Piriou, J.-L. Redelsperger, and P. M. Soares, 2004: Sensitivity of moist convection to environmental humidity. *Quart. J. Roy. Meteor. Soc.*, **130**, 3055–3080.

Emanuel, K. A., J. D. Neelin, and C. S. Bretherton, 1994: On large-scale circulations in convecting atmospheres. *Quart. J. Royal Meteor. Soc*, **120**, 1111–1143, doi:10.1002/qj.49712051902.

Fierro, A. O., J. M. Simpson, M. A. LeMone, J. M. Straka, and B. F. Smull, 2009: On how hot towers fuel the Hadley cell: An observational and modeling study of line-organized convection in the equatorial trough from TOGA COARE. *J. Atmos. Sci*., **66**, 2730–2746.

Fritsch, J. M., 1975: Cumulus dynamics: Local compensating subsidence and its implications for cumulus parameterization, *Pure Appl. Geophys*., 113, 851-867.

Giangrande S. E., S. Collis, J. Straka, A. Protat, C. Williams and S. Krueger, 2013: A summary of convective-core vertical velocity properties using ARM UHF wind profilers in Oklahoma, *J. Appl. Meteor. Climatol.,* **52**, 2278–2295

Heymsfield, G.M., L.Tian, A. J.Heymsfield, L. Li, and S.Guimond, 2010: Characteristics of deep tropical and subtropical convection from nadir-viewing high-altitude airborne Doppler radar. *J. Atmos. Sci.*, **67**, 285–308.

Johnson, R. H., T. M. Rickenbach, S. A. Rutledge, P. E. Ciesielski, and W. H. Schubert, 1999: Trimodal characteristics of tropical convection. *J. Climate*, **12**, 2397–2418.

Jorgensen, D. P., E. J. Zipser, and M. A. LeMone, 1985: Vertical motions in intense hurricanes. *J. Atmos. Sci*., 42, 839–856.

Keenan, T. D., K. Glasson, F. Cummings, T. S. Bird, J. Keeler, and J. Lutz, 1998: The BMRC/NCAR C-band polarimetric (CPOL) radar system. *J. Atmos. Oceanic Technol.*, **15**, 871–886.

Kuang Z., and Bretherton C.S., 2006: A Mass-Flux Scheme View of a High-Resolution Simulation of a Transition from Shallow to Deep Cumulus Convection. *J. Atmos. Sci.*, **63**, 1895 - 1909

Kumar, V. V., C. Jakob, A. Protat, P. T. May, and L. Davies, 2013a: The four cumulus cloud modes and their progression during rainfall events: A C-band polarimetric radar perspective. *J. Geophys. Res.*, DOI: 10.1002/jgrd.50640

Kumar, V. V., A. Protat, P. T. May, C. Jakob, G. Penide, S. Kumar, and L. Davies, 2013b: On the effects of large-scale environment and surface conditions on convective cloud characteristics over Darwin, Australia. *Mon. Wea. Rev*., **141**, 1358–1374.

Kumar V.V., Protat, A., Jakob, C., and May P. T., 2014: On atmospheric regulation of the growth of moderate to deep cumulonimbus in a tropical environment. *J. Atmos. Sci.*, **71**, 1105–1120.

Knupp K. R. and W. R. Cotton, 1985: Convective cloud downdraft structure' an interpretive survey, *Rev. of Geophy.* 23, 183-215.

LeMone, M. A., and E. J. Zipser, 1980: Cumulonimbus vertical velocity events in GATE. Part I: Diameter, intensity and mass-flux. *J. Atmos. Sci.*, **37**, 2444–2457.

Liu, C., and E. J. Zipser, 2005: Global distribution of convection penetrating the tropical tropopause. *J. Geophys. Res*., **110**, D23104, doi:10.1029/2005JD006063.

Marwitz, J. D., 1973: Trajectories within the weak echo regions of hailstorms. *J. Appl. Meteor.,* 12, 1174–1182.

May, P. T., and D. K. Rajopadhyaya, 1999: Vertical velocity characteristics of deep convection over Darwin, Australia. *Mon. Wea. Rev.,* **127**, 1056–1071.

May, P. T., A. R. Jameson, T. D. Keenan, P. E. Johnston, and C. Lucas, 2002: Combined wind profiler/polarimetric radar studies of the vertical motion and microphysical characteristics of tropical sea breeze thunderstorms. *Mon. Wea. Rev.*, **130,** 2228–2239.

May, P. T., J. H. Mather, G. Vaughan, C. Jakob, G. M. McFarquhXar, K. N. Bower, and G. G. Mace, 2008: The Tropical Warm Pool International Cloud Experiment. *Bull. Amer. Meteor. Soc*., **89**, 629–645.

Paluch, I. R., and C. A. Knight, 1984: Mixing and evolution of cloud droplet size spectra in a vigorous continental cumulus, *J. Atmos. Sci*., 41, 1801-1815.

Penide, G., V. V. Kumar, A. Protat, and P. T. May, 2013: Statistics of drop size distribution parameters and rain rates for stratiform and convective precipitation during the North Australian wet season. *Mon Wea. Rev.*, doi: 10.1175/MWR-D-12-00262.1

Petch, J., A. Hill, L. Davies, A. Fridlind, C. Jakob, Y. Lin, S. Xie, and P. Zhu, 2014: Evaluation of intercomparisons of four different types of models simulating TWP-ICE *Quart. J. Roy. Meteorol. Soc.***,** **140**, 826–837

Pope, M., C. Jakob, and M. Reeder, 2009: Regimes of the North Australian Wet Season. *J. Climate*, **22**, 6699–6715.

Protat, A., and C. R. Williams, 2011: The accuracy of radar estimates of ice terminal fall speed from vertically pointing Doppler radar measurements. *J. Appl. Meteor. Climatol.*, **50**, 2120–2138.

Protat, A., and I. Zawadzki, 1999: A variational method for real-time retrieval of three-dimensional wind field from multiple-Doppler bistatic radar network data. J. Atmos. Oceanic Technol., 16 (4), 432-449.

Randall, D. A., and Coauthors, 2003: Confronting models with data - The GEWEX Cloud Systems Study. *Bull. Amer. Meteor. Soc*, **84**, 455–469.

Redelsperger, J. -L., D. B. Parsons, and F. Guichard, 2002: Recovery processes and factors limiting cloud-top height following the arrival of a dry intrusion observed during TOGA COARE. *J. Atmos. Sci.*, **59**, 2438–2457.

Roode, S. R.D., A.P. Siebesma,H. J. J. Jonker and Y. D. Voogd, 2012: Parameterization of the vertical velocity equation for shallow cumulus clouds. *Mon. Wea. Rev.*, **140**, 2424–2436.

Steiner, M., R. A. Houze Jr., and S. E. Yuter, 1995: Climatological characterization of three-dimensional storm structure from operational radar and rain gauge data. *J. Appl. Meteor.*, **34**, 1978–2007.

Takemi, T., O. Hirayama, and C. Liu, 2004: Factors responsible for the vertical development of tropical oceanic cumulus convection. *Geophys. Res. Lett.*, **31**, L11109, doi:10.1029/ 2004GL020225.

Williams,C.R., 2012:Vertical airmotion retrieved from dual-frequency profiler observations. *J. Atmos. Oceanic Technol.*, **29,** 1471–1480.

Xie, S., R. T. Cederwall, and M. Zhang, 2004: Developing long-term single-column model/cloud system - resolving model forcing data using numerical weather prediction products constrained by surface and top of the atmosphere observations. *J. Geophys. Res.*, **109**, DOI: 10.1029/2003JD004045.

Yanai, M., S. Esbensen, and J. Chu, 1973: Determination of bulk properties of tropical cloud clusters from large-scale heat and moisture budgets. *J. Atmos. Sci*., **30**, 611–627.

Zhang, M. and J. Lin, 1997: Constrained variational analysis of sounding data based on column-integrated budgets of mass, heat, moisture, and momentum: Approach and application to ARM measurements. *J. Atmos. Sci*., **54**, 1503–1524.

Zipser, E. J., 2003: Some view on ‘‘hot towers’’ after 50 years of tropical field programs and two years of TRMM data. *Cloud Systems, Hurricanes, and the TRMM. Meteor. Monogr., No. 51, Amer. Meteor. Soc.,* 49–58.

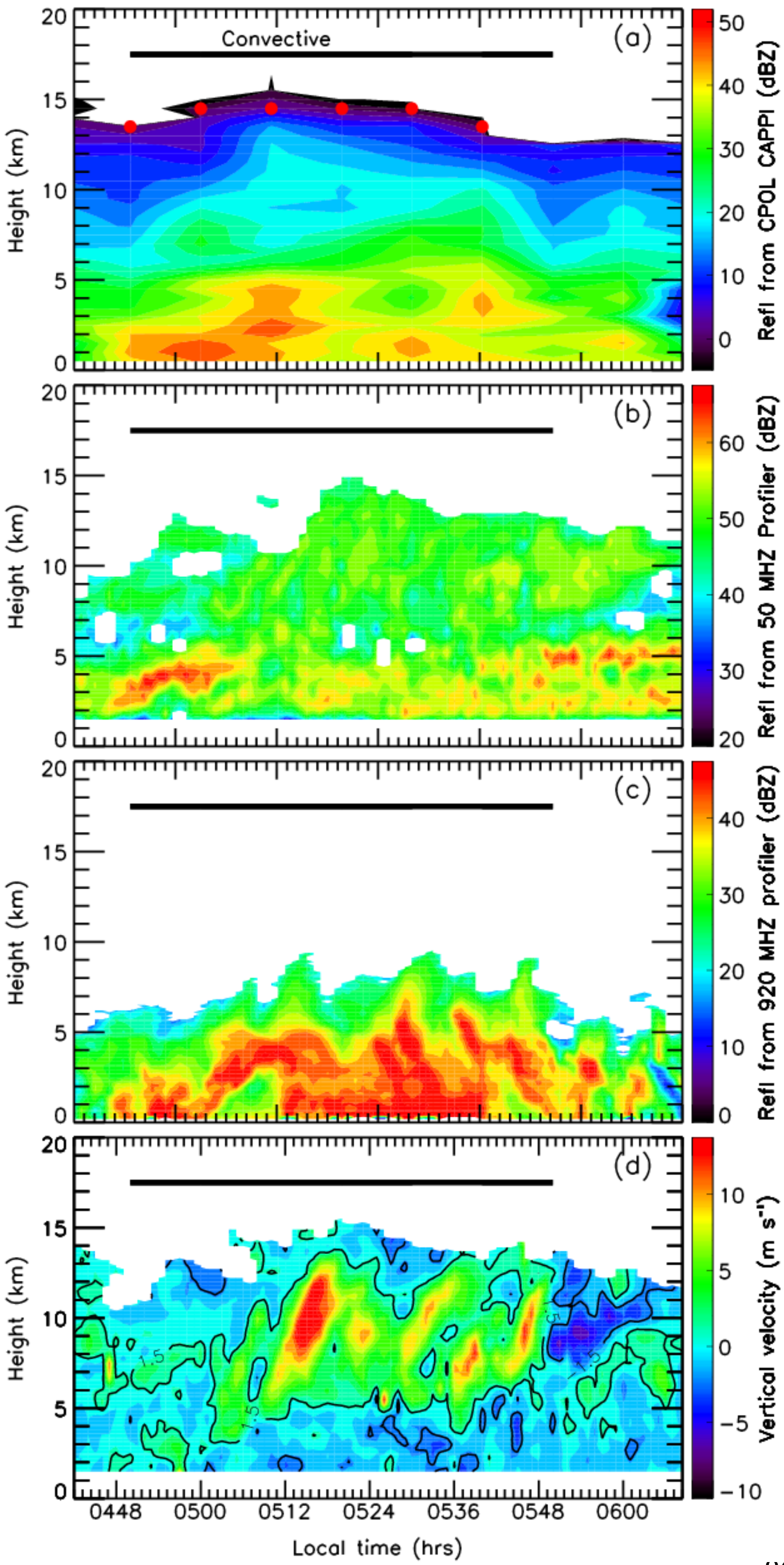

Figure 1: Overshooting convection captured by the wind profiler around 0500 LT on 21st March 2006. a) Time-height section of the Darwin C-band polarimetric (CPOL) radar reflectivity collocated with wind profiler site. CPOL data used here is from volumetric mode,

where the data was collected over 10 mins intervals. The CPOL data was gridded in height steps of 0.5 km. The red line is the 0-dBZ ETH of Steiner classified convective columns; ETH of stratiform columns are not important to this study. The length of convective interval in all panels is highlighted by the thick horizontal line. b)-d) Reflectivity from the 50 MHz wind profiler, reflectivity from the 920 MHz wind profiler, vertical velocity (v) obtained using the combination of the 50 and 920 MHz Doppler velocities, respectively. The profiler data were displayed in using its primary resolution in bins of 1 min in time and 0.1 km bins in height.

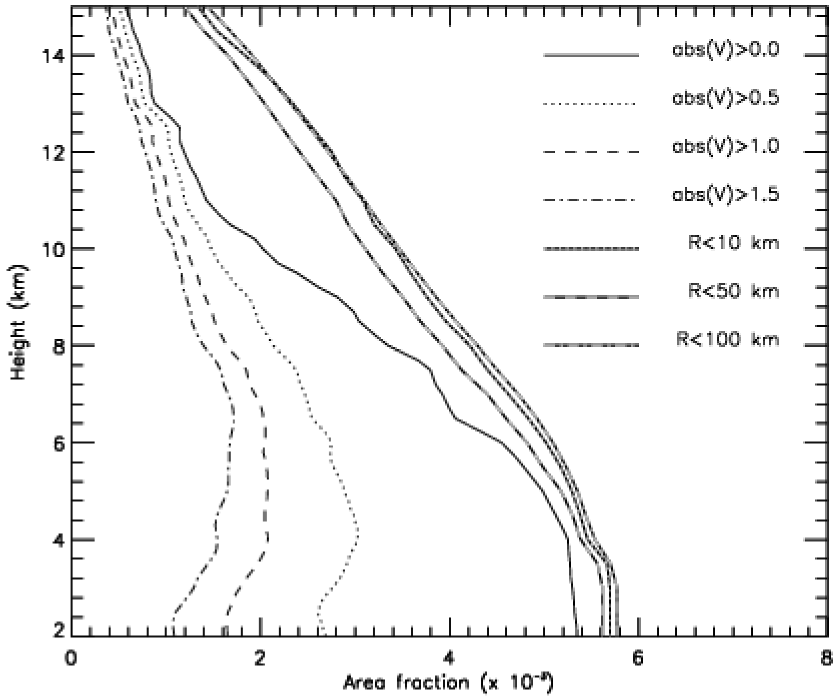

Figure 2: The two wet-season mean profile of convective area fractions using vertically pointing observations from the wind profiler and volumetric observation from CPOL. As explained in the text, wind profiler area fractions were extracted by applying the “time approach” for different absolute vertical velocity threshold ranging from 0 to 1.5 m s^{-1} in steps of 0.5 m s^{-1}. The area fractions from CPOL is extracted using the “space approach” for different circular region of radius ranging from 10 to 100 km centred over the wind profiler site.

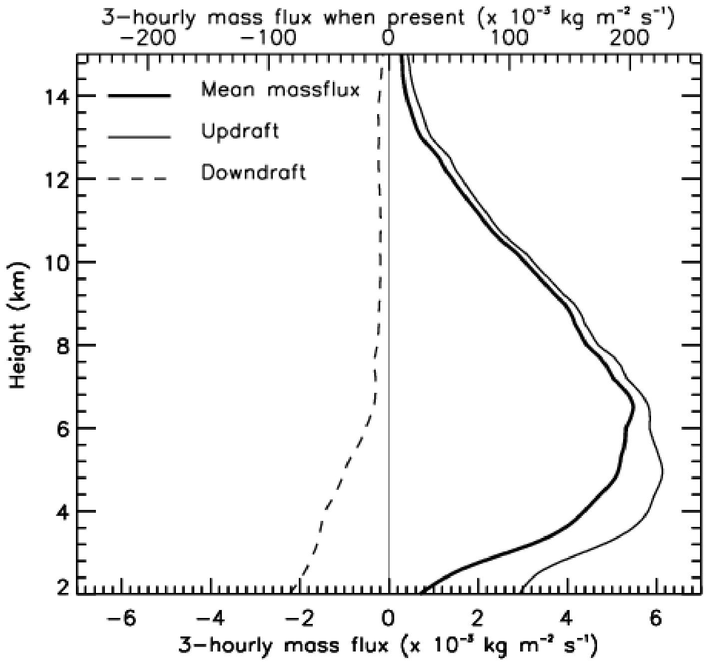

Figure 3: Two wet-season mean vertical profile of mass flux (thick curve), updraft (thin curve) and downdraft (dashed curve). Mass flux values were extracted using the GCM-type definition for mass flux considering all cumulus clouds occurring over a large area. Secondary x axis represents mass flux values provided there was at least one cumulus cloud in the 3-hour window. A 3-hour bin corresponds to nearly 60 km in distance, assuming the atmospheric flow speed is 5 m s^{-1}.

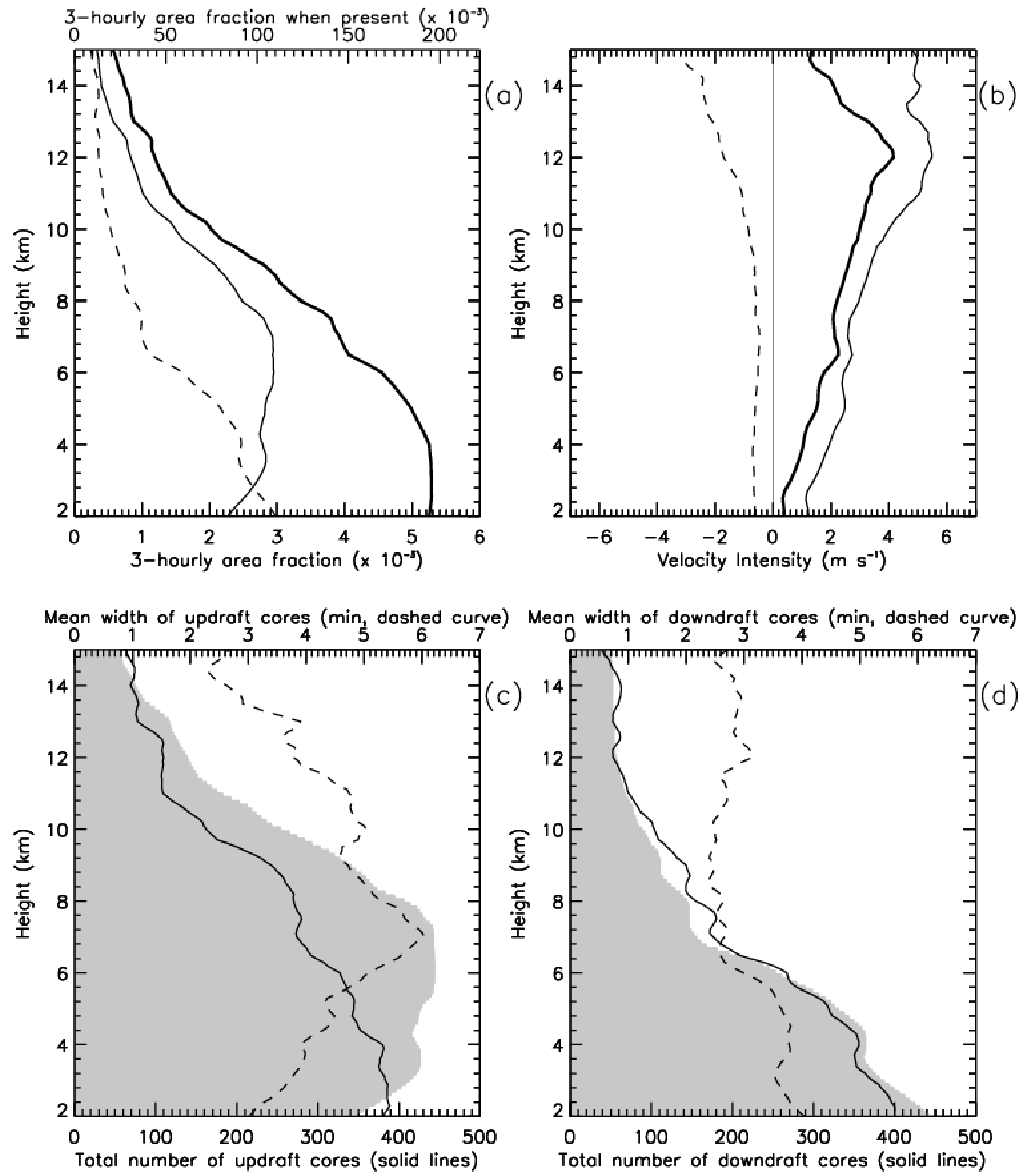

Figure 4: The same format as Fig.3 and shows mean profiles of the (a) mean area fractions, (b) vertical velocity, c) cumulative count of updraft cores (solid curve) and mean width (dashed curve) - product of these two factors equates to upward area fraction (shaded) and d) is the same as (c) and shows the characteristics of downdrafts.

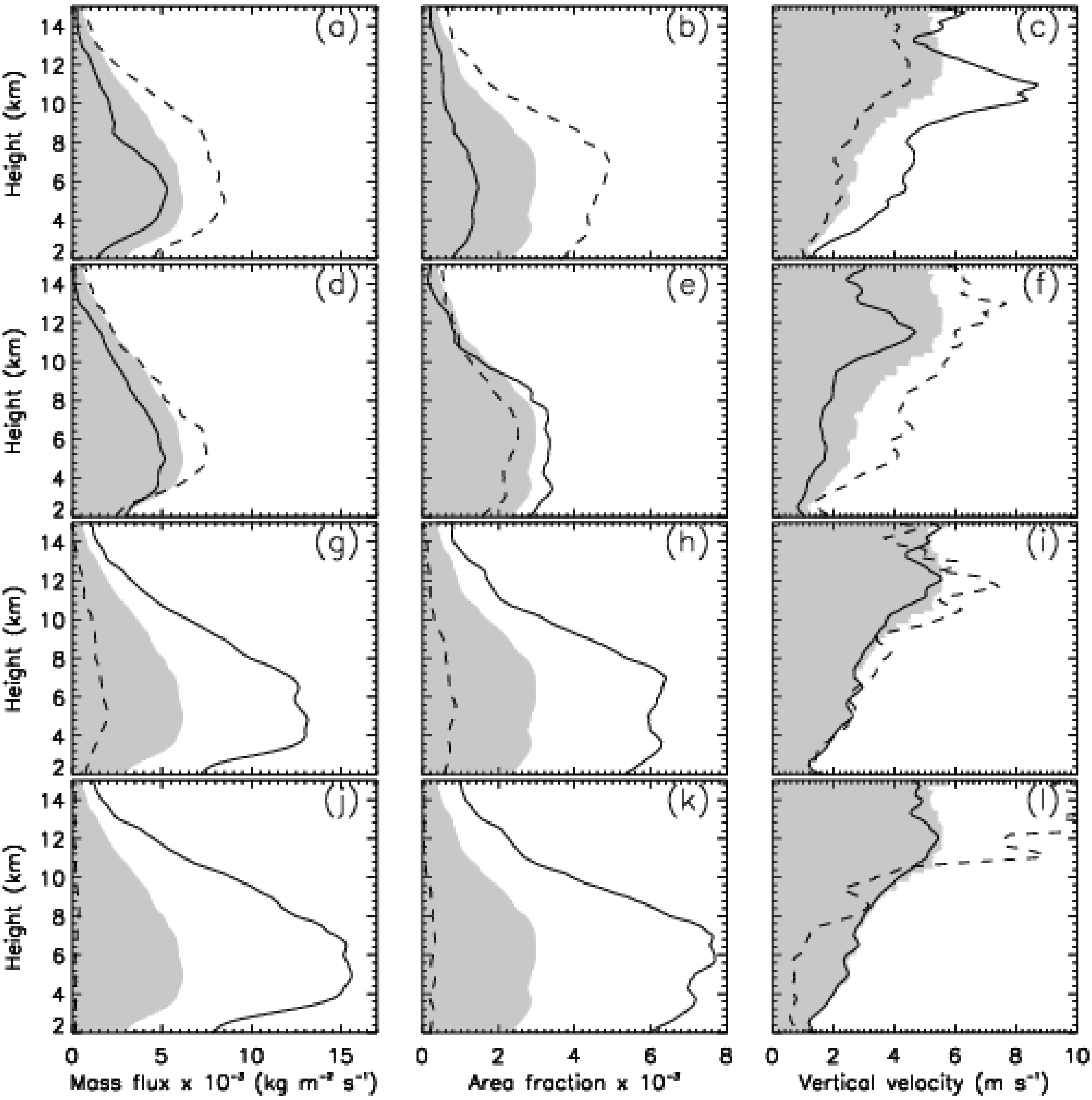

Figure 5: Effect of 0–5 km relative humidity ($RH_{0\text{-}5}$, top panels), CAPE (second panels), CIN (third panels) and 500 HPa large-scale vertical velocity (ω_{500}) on updraft mass flux (left column), upward area fraction (middle column) and upward vertical velocity intensities (right column). The shaded region is the overall updraft means without applying any environmental sorting. The solid and dotted line in each figure corresponds to lower and upper terciles of the background condition. The tercile boundaries are in table 1.

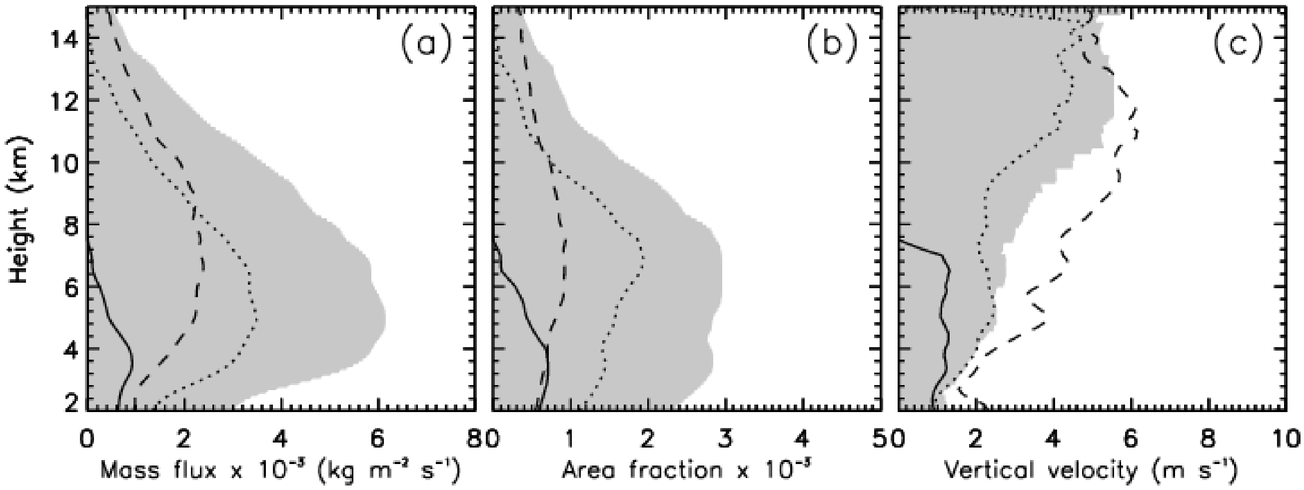

Figure 6: Contribution to (a) updraft mass flux, (b) upward area fraction, and (c) vertical velocity from congestus (solid), deep (dotted) and overshooting (dashed) cumulus clouds. The shaded region represents is due to all the cumulus cloud modes.

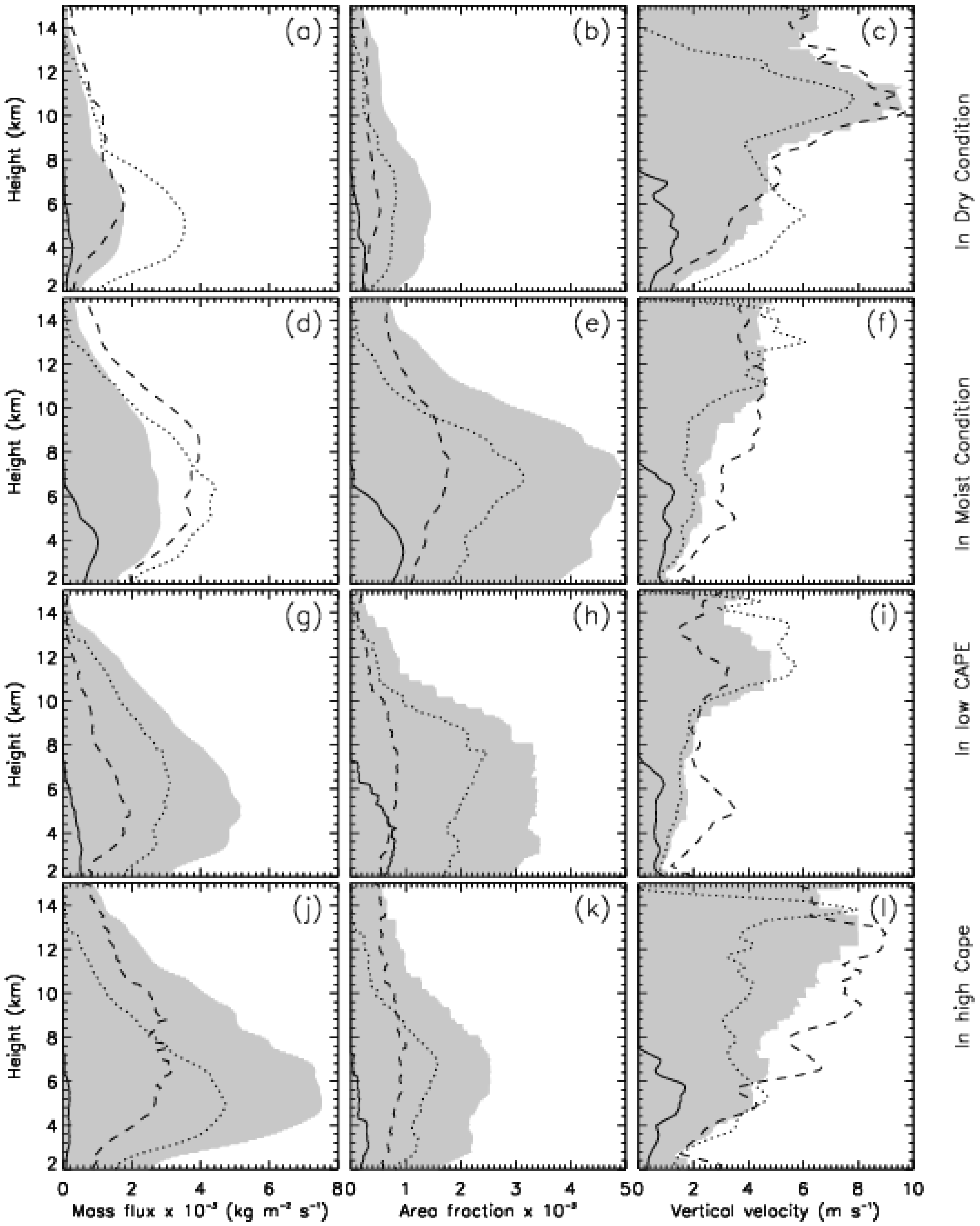

Figure 7: The same format as Fig. 6 and shows the mean response of the three cumulus modes in dry conditions (top panels), moist condition (second panels), low CAPE condition (third panels) and high CAPE condition (bottom panels).

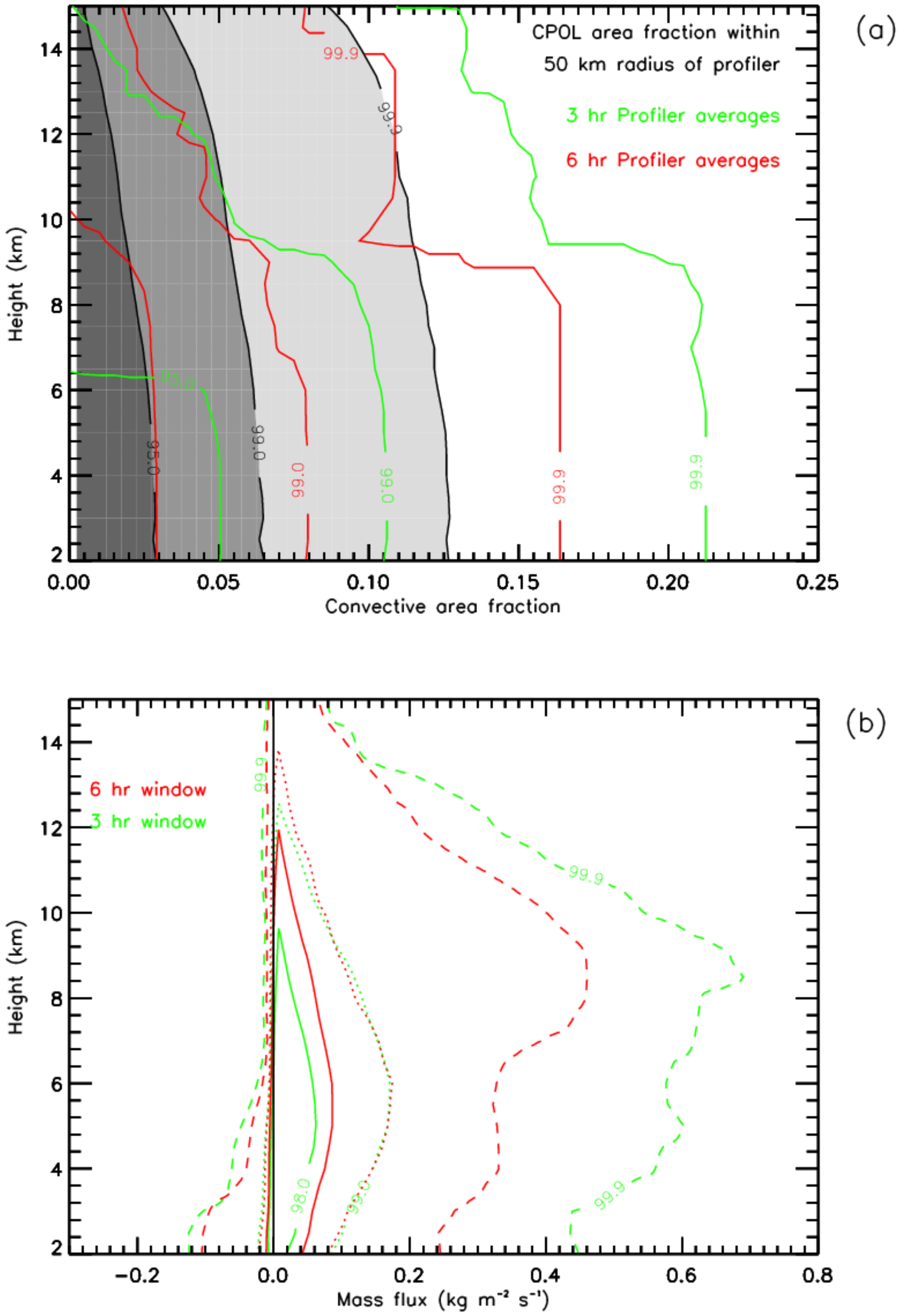

Figure 8: a) 2D cumulative probability distribution of convective area fraction from CPOL over the circular region of radius 50 km centred at the profiler site (shaded) and convective area fraction from wind profiler observations over discrete time intervals of 3 hours (green) and 6 hours (red). b) The same as a) and shows the mass flux from wind profiler.

Table 1: The two wet-season occurrence frequency of congestus, deep and over-shooting clouds, and separately for four environment background conditions

Environmental Condition	**Total of the 1-min wind profiler scans**			
	Congestus (CTH < 7 km)	Deep (7 km < CTH < 15 km)	Over-shooting (CTH > 15 km)	All cumulus clouds
0-5 km RH ≤68%	145	196	148	489
0-5 km RH 68%-82%	228	557	184	969
0-5 km RH ≥82%	292	741	337	1370
CAPE ≤365 J kg^{-1}	251	620	184	1055
CAPE 365 – 747 J kg^{-1}	305	540	222	1067
CAPE ≥747 J kg^{-1}	109	334	263	706
CIN ≤30 J kg^{-1}	527	1030	512	2069
CIN 30 – 62 J kg^{-1}	78	346	127	551
CIN ≥62 J kg^{-1}	60	118	30	208
ω_{500} ≤ -1.82 hPa $Hour^{-1}$	485	1232	649	2366
ω_{500} -1.82 to 1.24 hPa $Hour^{-1}$	109	176	10	295
ω_{500} ≥ 1.24 hPa $Hour^{-1}$	71	86	10	167
All	665	1494	669	2828